Eur. Phys. J. A **9**, 463–472 (2000)

THE EUROPEAN PHYSICAL JOURNAL A

© Società Italiana di Fisica
Springer-Verlag 2000

Decay of ^{83}Sr and level structure of ^{83}Rb

Shen Shuifa[1,2,a], Yu Xiaohan[2], Shi Shuanghui[2], Gu Jiahui[2], Liu Jingyi[2], Li Yan[2], and Zhu Zhiyuan[1,2]

[1] Shanghai Institute of Nuclear Research, Chinese Academy of Sciences, Shanghai 201800, People's Republic of China
[2] CCAST (World Lab.), P.O. Box 8730, Beijng 100080, People's Republic of China

Received: 17 November 1999 / Revised version: 17 September 2000
Communicated by D. Guerreau

Abstract. The excited states of the ^{83}Rb nucleus were investigated in radioactive decay of ^{83}Sr. The level scheme was established and for a number of levels spin-parity assignments are suggested on the basis of $\log ft$ values and γ-branching ratios. Combining with the high-spin states observed by the in-beam γ-ray spectroscopy of a previous decay work, the structure of the excited states of ^{83}Rb is discussed in the framework of the projected shell model.

PACS. 23.20.Lv Gamma transitions and level energies – 27.50.+e $59 \leq A \leq 89$ – 21.60.Cs Shell model

1 Introduction

The neutron-deficient ^{83}Rb nucleus having several protons and neutrons in the unfilled shells exhibit a quite complex structure of excited states. Any of the simple models based on the known nucleon coupling schemes fails in the description of this nucleus. The possibility for protons and neutrons to occupy the same orbitals may further complicate the situation as the short-range proton-neutron interaction is expected to become quite important.

Nuclei around $A = 80$ have been studied extensively using γ-ray spectroscopy, since they exhibit abundant nuclear structure information. During an examination of Rb nuclei, we found that some contradictions remain in the low-energy and low-spin part of the ^{83}Rb level scheme. Detailed information on states with low-spin values and low excitation energies can be obtained using γ-ray (and conversion electron) spectroscopy following radioactive decay. The β decay of ^{83}Sr ($T_{1/2} = 32.41$ h) presents an excellent way to get information about the low-energy levels of ^{83}Rb. The decay of ^{83}Sr was previously studied by Etherton *et al.* [1], Broda *et al.* [2], and Grütter [3]. Many inconsistencies (for example, many γ-ray energies mismatch the level differences by more than three standard deviations, 16 γ-rays which were assigned to the decay of ^{83}Sr were left out of the decay scheme, and many transitions hidden in 12 unresolved γ-ray multiplets have been located in two or more places in the decay scheme) appear within the decay scheme [4] as deduced from the experimental data due to poor energy resolution, low statistics or a lack of sufficient coincidence data. Thus, it is necessary to reinvestigate the decay of ^{83}Sr. Because better experimental techniques are now available, this decay has been remeasured in order to improve the ^{83}Rb level scheme at low spins and to reveal a clearer connection with the high-spin scheme proposed by Gast *et al.* [5], and Döring *et al.* [6]. Particular attention has been paid to the many formerly unresolved γ-ray multiplets.

In this work the results of our investigation on the ^{83}Rb isotope in radioactive decay are presented. Preliminary results of this work have been published elsewhere [7]. In section 2 the experimental procedures are presented. Section 2.1 reports on the preparation of the ^{83}Sr source. Sections 2.2 and 2.3 report on the results of singles and coincidence measurements and the model independent level scheme construction, β decay branching ratios and spin-parity assignments, and in section 3 the interpretation of the level scheme in the framework of the projected shell model (PSM) is presented.

2 Experimental procedure

2.1 Source

The ^{83}Sr sources were produced through the ^{85}Rb $(\mathrm{p}, 3\mathrm{n})^{83}$Sr reaction by irradiating a high-purity RbCl powder ($0.2\,\mathrm{g/cm^2}$) with beams of 27.1 MeV protons ($I \approx 10\,\mu$A), obtained from the variable-energy cyclotron ($K = 40$) at the Shanghai Institute of Nuclear Research (SINR). Three different targets were irradiated every three days one-by-one. Natural RbCl powder was backed with a 0.5 mm Al plate and covered by a 30 μm aluminium foil. The chemical procedure for the extraction of the Sr activity from the target material was started after a waiting period of ~ 20 h at the end of the irradiation and lasted about 10 h. The target was dissolved in diluted nitric acid,

[a] e-mail: ssh@sinr.ac.cn

containing some of the Sr^{2+} carriers. $SrSO_4$ was precipitated from the solution by the addition of concentrated H_2SO_4. The precipitate was washed with a diluted H_2SO_4 solution and filtered with a chimney filter to prepare the counting sources. However, very small amounts of ^{85}Sr, ^{83,84}Rb, and ^{131}Ba contaminants remained in the sources.

2.2 Experimental methods

2.2.1 Singles spectrum measurement

The singles spectra were measured with a low background Compton-suppressed high-purity Ge detector with a volume of 130 cm^3 and a resolution of 1.9 keV at 1332 keV. Spectra with and without anti-Compton suppression were recorded. The sources were placed at a distance of 22 cm from the detector and the counting rate was controlled to be less than 2500 counts per second (cps) so that the cascade or random summing effect was negligible. The measured energy region was between 30 and 2650 keV and the background counting rate in this energy region was 0.7 cps. Calibration measurements were performed for one hour both before and after two hours of measurements for the first ^{83}Sr source to obtain the energy of strong peaks. Then each of the three ^{83}Sr sources was measured for about three days which were divided into 9 time bins of 20000 s each. Since the drifts of all measured spectra were very small (< 0.06 keV), a series of summed spectra was obtained by adding the above-mentioned spectra directly. These summed spectra were analyzed carefully with a peak-fitting programme. The energies of strong peaks were taken as calibration standards for weak peaks identified from the summed spectra. The analysis of the half-life of each resolved peak was performed in order to roughly discriminate γ-rays originating from the decay of ^{83}Sr against those from background and contaminants. The energy and relative efficiency calibrations were performed with ^{152}Eu and ^{133}Ba sources placed at the target position. X-rays of ^{152}Eu were also used [8]. The relative intensities of the γ-rays were normalized to the intensity of the 762.6 keV transition which was set to $I_\gamma = 100$. An additional measurement of the relative intensity of the 511 keV annihilation radiation was performed from which the total β^+ decay intensity can obtained for a ^{83}Sr source sandwiched between 3 mm of lead to produce total annihilation in order to determine the (β^++EC) branching ratio to the ^{83}Rb ground state. The result is $I(511\gamma) = 160 \pm 5$ by assuming $I(762\gamma) = 100$.

2.2.2 Coincidence measurement

Coincidence measurements were made using two high-purity Ge detectors oriented at 90 °, one of which was a planar Ge detector (GMX-20190) with 20% efficiency and 1.85 keV resolution at 1332 keV and placed 10 cm from the target, the other was a coaxial Ge detector (GEM-50195) with 50% efficiency and 2.0 keV resolution at 1332 keV and placed 15 cm from the target. The data were stored in an event-by-event recording mode on the computer's hard disk. For each event one time and two energy parameters of 8192 channels were included. The fast-slow coincidence circuit had a time resolution of about 20 ns when gated by the ^{60}Co full energy peaks. For low-energy transitions it can be much larger. About 7.0×10^6 events were stored. The reconstruction of coincidence spectra was performed off-line. For each gate, a gross spectra without random coincidence and background correction and a background spectra were both obtained. Coincidence relationships were determined by comparing this pair of spectra. Almost all transitions determined in singles spectra were observed in coincidence spectra too. On the other hand, several weak peaks which could not be separated in singles spectra were also identified in coincidence spectra. Selected results for some examples of coincidence spectra are shown in fig. 1.

2.3 Experimental results

The present investigation of the ^{83}Sr decay provides an extension of the information concerning this decay. Approximately 190 transitions including 94 new transitions and 19 new levels were assigned to ^{83}Rb, based on their measured half-life and/or observation in coincidence with well-known transitions. A decay scheme has been constructed consisting of 41 excited states and 180 transitions in ^{83}Rb. Additional new information has been obtained on γ-ray branching ratios, $\log ft$ values, spins and parities.

The proposed decay scheme of ^{83}Sr shown in fig. 2 is based essentially on the results of γ-γ-t coincidence measurements performed with two HpGe detectors. The coincidences are indicated by solid circles, and open circles mean that the coincidence relations are uncertain. This decay scheme incorporates all the observed γ-transitions except seven relatively weak ones. These seven new γ-rays were assigned to the decay of ^{83}Sr based on their measured half-life, but they could not be placed in the decay scheme. Their energies and relative intensities are listed in table 1.

Some levels from the previous decay scheme have not been taken over in the new decay scheme because they obtained no support from the coincidence data. However, most of the γ-rays previously connected with these levels could be placed in the new decay scheme according to the coincidence and energy sum relations. The energies of these levels are 760.0, 1044.1, 1054.5, 1085.5, 1808.4, 2020.2, 2147.3, and 2178.2 keV.

The intensity balance performed for individual levels and the intensity of the 511 keV annihilation peak were employed to determine the β-branches to the ground and excited states of ^{83}Rb, for which adequate $\log ft$ values were obtained using the decay energy $Q_{\rm EC} = 2256 \pm 10$ keV [9]. By combining the $\log ft$ values and the de-excitation modes of the observed states of ^{83}Rb, as well as the results of the in-beam experiments performed by Gast *et al.* [5] and Döring *et al.* [6], a number of unambiguous spin-parity assignments were made which are also given in fig. 2.

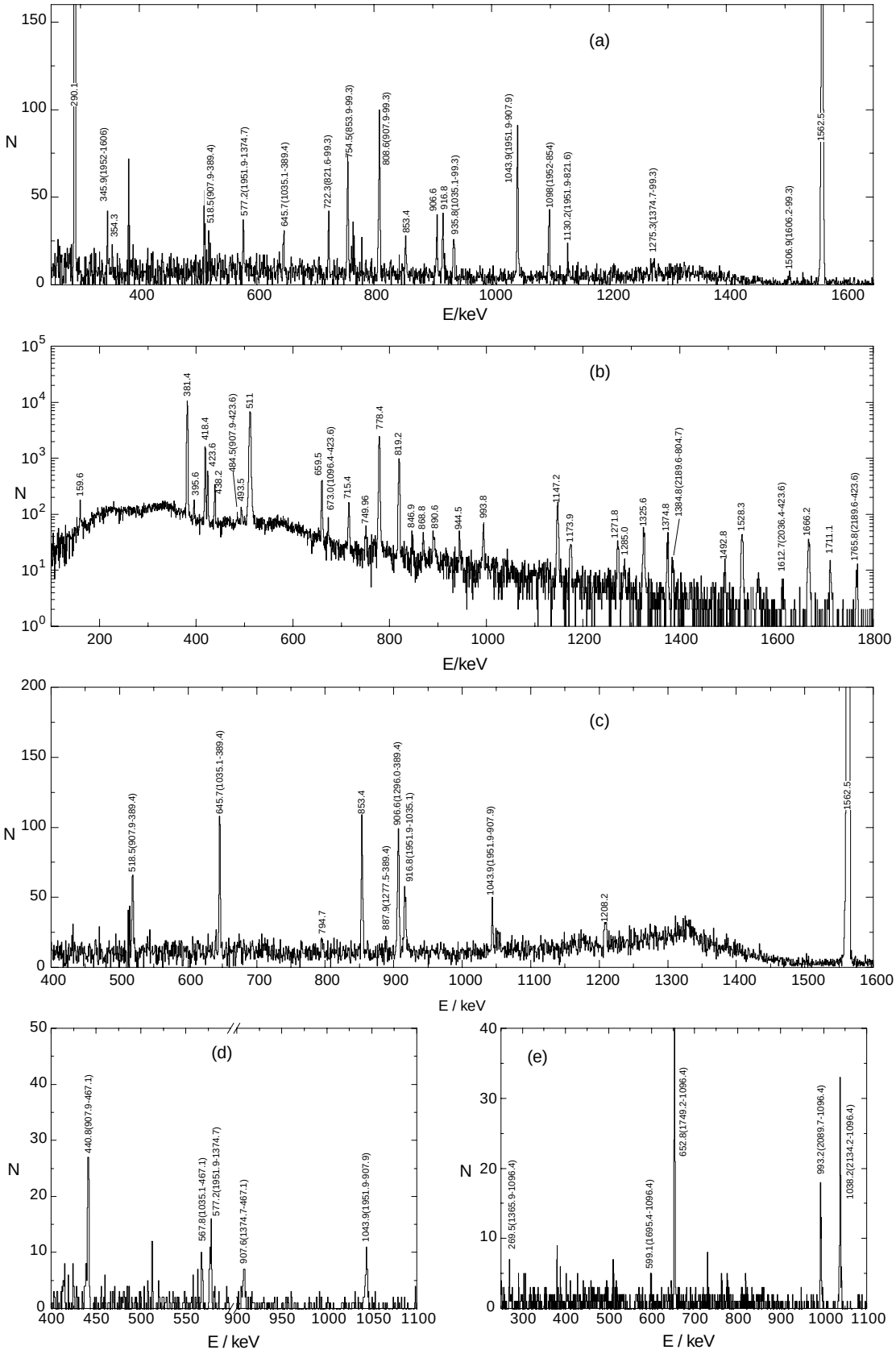

Fig. 1. Some examples of coincidence spectra gated by (a) 94 keV, (b) 380–382 keV, (c) 389 keV, (d) 462 keV, (e) 1054 keV, (f) 559 keV, (g) 749–755 keV, (h) 1044 keV γ-rays following the decay of ^{83}Sr, respectively. The numbers in parentheses denote the placement.

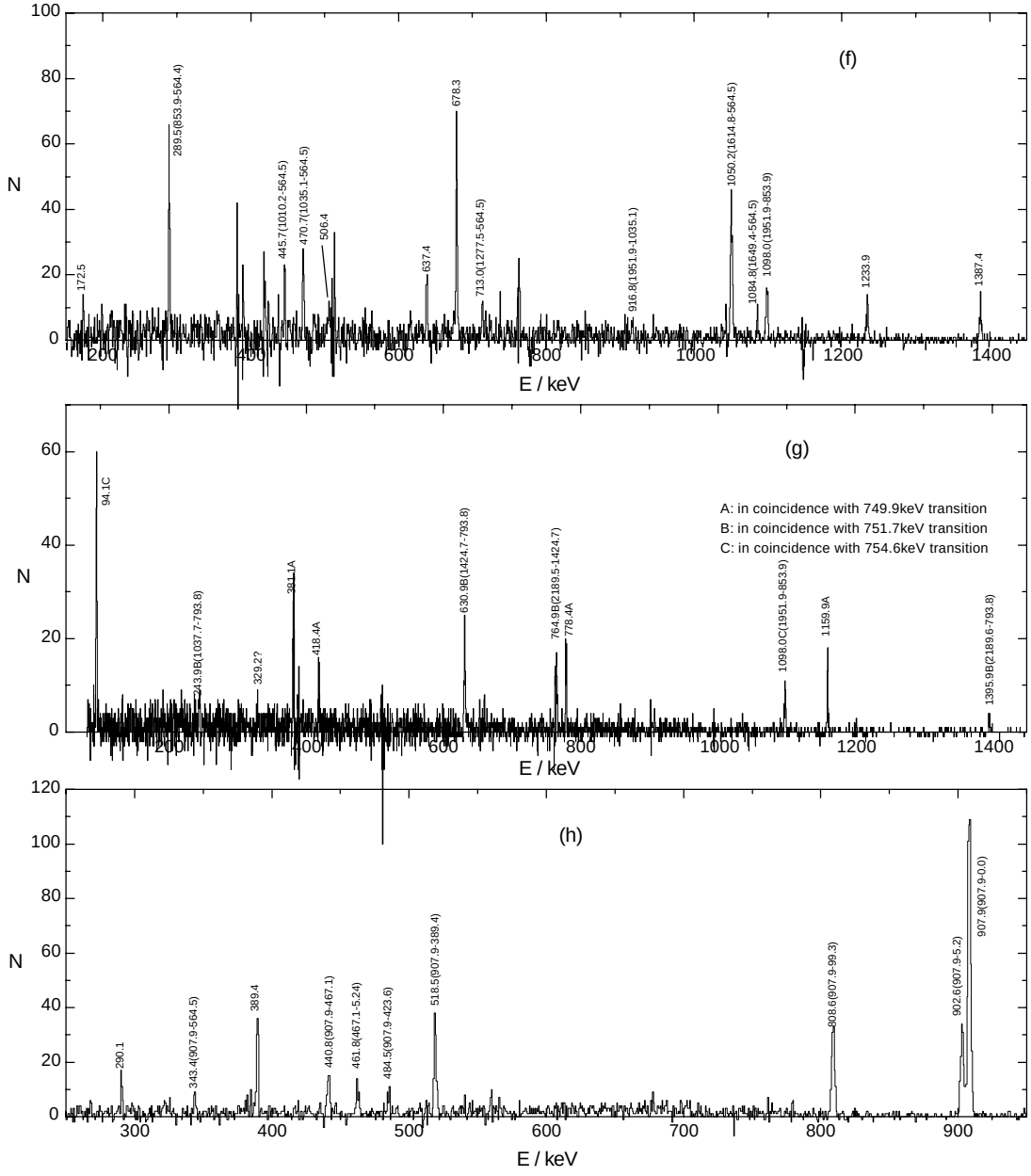

Fig. 1. Continued.

Table 1. Energies and relative intensities of transitions assigned to the decay of ^{83}Sr but not placed in the decay scheme.

E/keV	758.2	856.8	1498.6	1608.9	1709.4	1777.9	1873.7
Relative intensity	0.08	0.017	0.005	0.007	0.013	0.082	0.108

There are a total of 27 levels which have not been observed before, or have been observed in previous work but are not confirmed in the present work, or for which the population and depopulation mode or spin-parity assignments have been revised significantly with respect to previous works. As examples, three new levels at 793.8, 853.9, and 907.9 keV are briefly discussed.

793.8 keV *level.* A level at 794.2 keV was first observed by Gast *et al. via* the (^{6}Li,3nγ) reaction [5]. This level is depopulated by a 751.9 keV transition to the first $9/2^+$ level. A J^π value of $13/2^+$ was assigned from angular distribution and reaction results. With such a J^π value, this level should not be populated by $\beta^+ + \mathrm{EC}$ decay. In the present work, the 753.3 keV line measured by Broda *et al.* [2] was proved to have three components in which the most intense component is the 751.7 keV transition. This transition is observed in coincidence with the 630.9, 764.8, and 1395.9 keV lines. Both of the sum of the 751.7

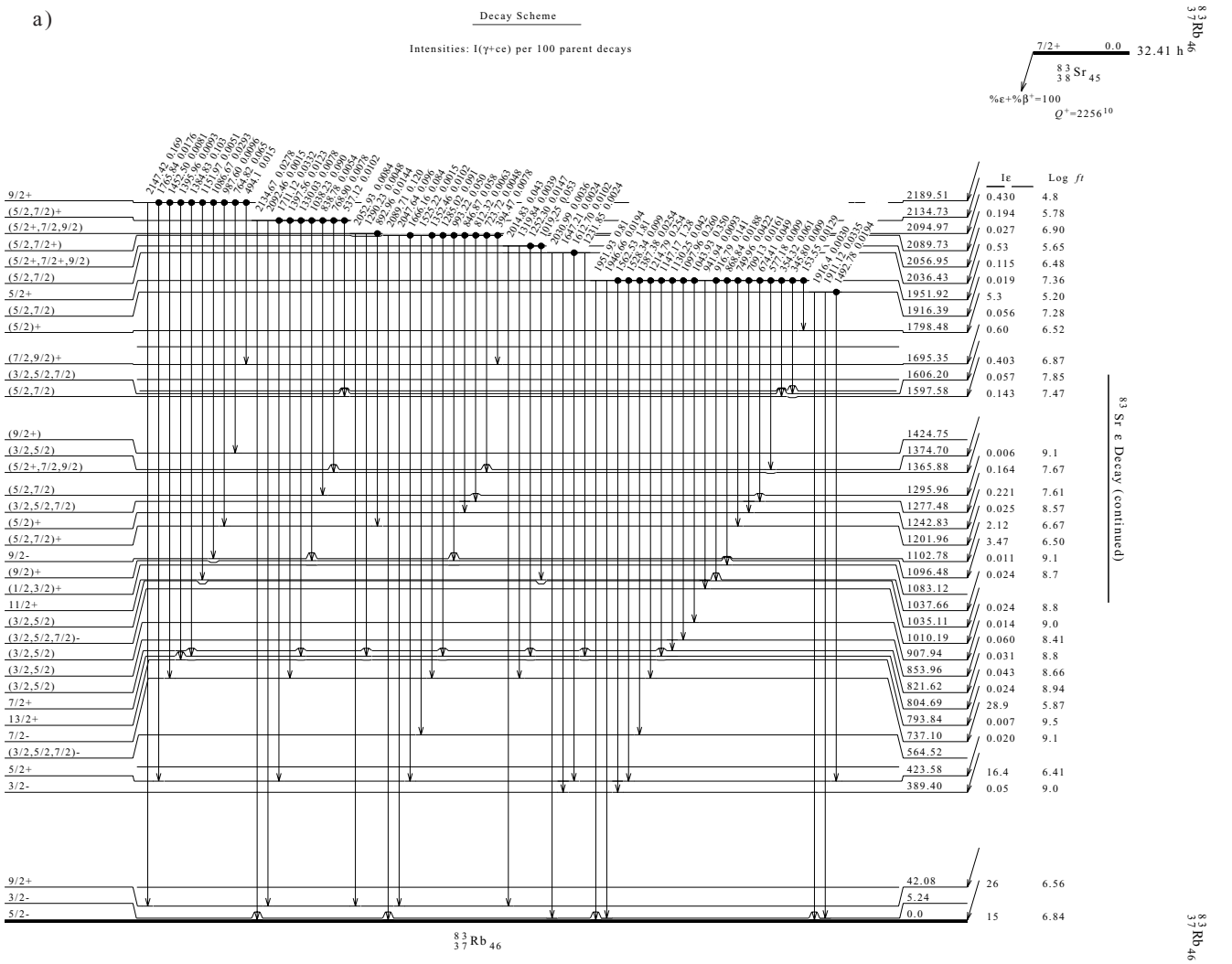

Fig. 2. The proposed decay scheme of ^{83}Sr established in the present experiment.

and 1395.9 keV transitions and of the 751.7, 630.9, and 764.8 keV transitions are compatible with the 2147.4 keV transition. Therefore, a level at 793.84 keV is proposed. The measured log ft value of 9.5 is not in agreement with the spin-parity assignment given by Gast *et al.* [5]. The origin of this discrepancy may be possible weak γ transitions which may populate this level and have not been identified in the present work. So $J^\pi = 13/2^+$ is adopted.

853.9 keV *level.* The 1098.0 keV transition shows coincidence with 853.9, 848.7, 754.6, 559.3, 564.5, and 289.5 keV transitions. The 289.5 keV transition was observed in coincidence with the 559.3 keV transition, and the 94.1 keV transition was observed in coincidence with the 754.6 keV transition. Therefore, a new level at 853.9 keV is proposed. The 1098.0 keV transition depopulates the well-known 1951.9 keV level and thus the previous placement of this transition is incorrect. Considering the log ft value and γ selection rules, the values $(3/2, 5/2^-)$ are proposed.

907.9 keV *level.* The 1043.9 keV transition feeding this level is observed in coincidence with the lines at 907.9, 902.6, 808.6, 518.5, and 389.4 keV. In addition, the 389.4 keV transition shows coincidence with the 518.5 keV transition, and the 94.1 keV transition shows coincidence with the 808.6 keV transition. Therefore a new level at 907.9 keV is proposed. Values $(3/2, 5/2^-)$ are suggested for the same reason as for the 853.9 keV level.

3 Discussion

3.1 Summary of the theory

The projected shell model [10–13] employed in this paper is a microscopic theory, which solves the many-nucleon system fully quantum mechanically. The ansatz for the angular-momentum-projected wave function is given by

$$|IM\rangle = \sum_k f_k \hat{P}^I_{MK_k} |\varphi_k\rangle, \qquad (1)$$

where k labels the basis states. $\hat{P}^I_{MK}$ is the angular-momentum projection operator which is explicitly given

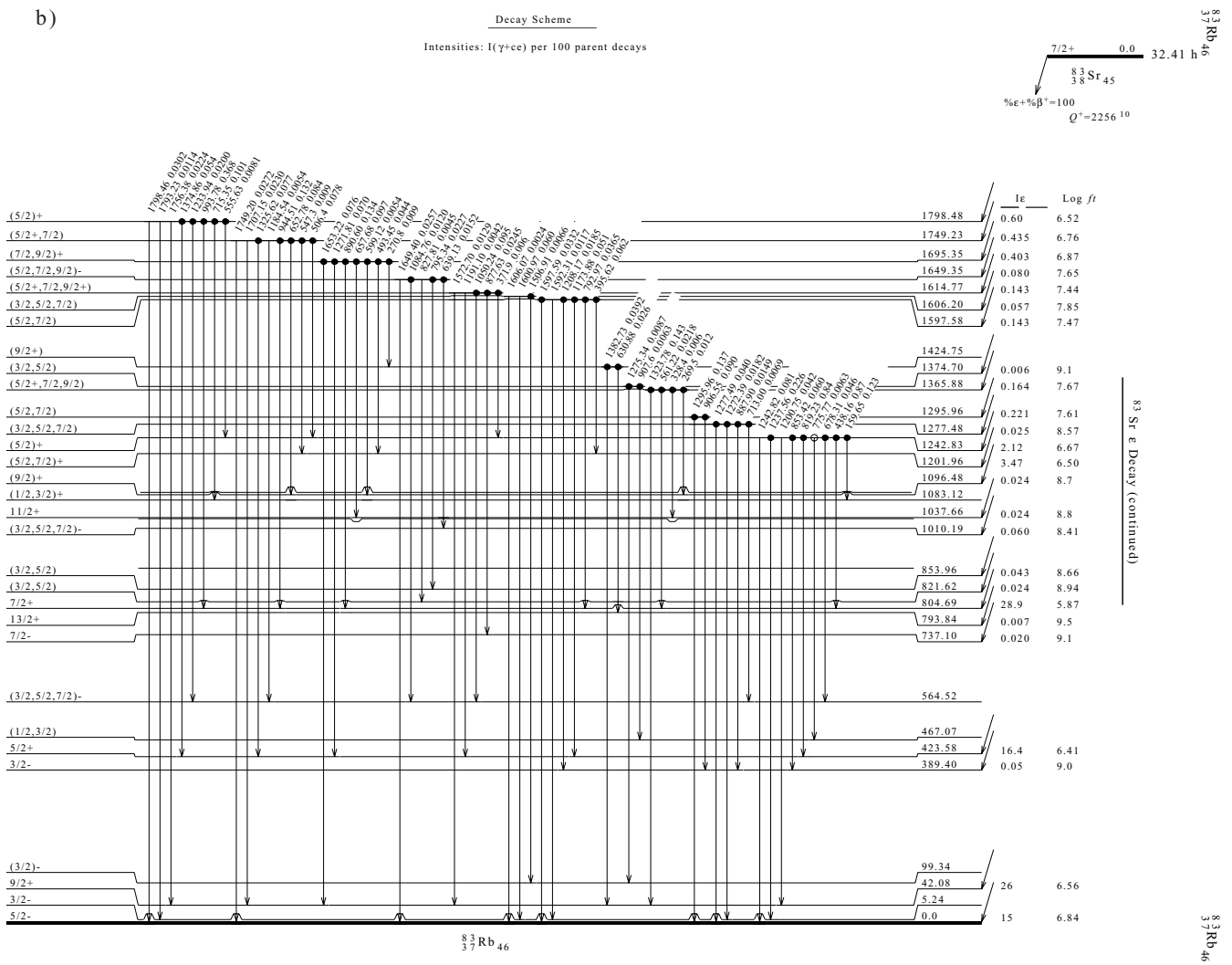

Fig. 2. Continued.

in ref. [10]. Acting on an intrinsic state $|\varphi_k\rangle$, the operator $\hat{P}^I_{MK}$ generates states of good angular momentum, thus restoring the necessary rotational symmetry violated in the deformed mean field. In this way the new shell model basis is constructed in which the Hamiltonian is diagonalized, this shell model basis taken in the present work is as follows:

$$\hat{P}^I_{MK}|\varphi_k\rangle. \tag{2}$$

The basis states $|\varphi_k\rangle$ are spanned by the set

$$\left\{a^+_{\rm p}|0\rangle, a^+_{\rm n_1}a^+_{\rm n_2}a^+_{\rm p}|0\rangle\right\}, \tag{3}$$

for odd proton nuclei. $|0\rangle$ denotes the quasiparticle vacuum state and $a^+_{\rm n}(a^+_{\rm p})$ is the neutron (proton) quasiparticle creation operator for this vacuum; the index $\rm n_{1(2)}(p)$ runs over selected neutron (proton) quasiparticle states and k in eq. (1) runs over the configuration of eq. (3). The vacuum is obtained by diagonalizing a deformed Nilsson Hamiltonian [14] followed by a BCS calculation. In the calculations, we have used three major shells, *i.e.*, $N = 2, 3,$ and 4 ($N = 2, 3,$ and 4) for neutrons (protons) as the configuration space.

In this work we have used the Hamiltonian [13]

$$\hat{H} = \hat{H}_0 - \frac{1}{2}\chi\sum_\mu \hat{Q}^+_\mu\hat{Q}_\mu - G_{\rm M}\hat{P}^+\hat{P} - G_{\rm Q}\sum_\mu \hat{P}^+_\mu\hat{P}_\mu, \tag{4}$$

where $\hat{H}_0$ is the spherical single-particle shell model Hamiltonian, $\hat{Q}_\mu$ is the quadrupole moment operator, $\hat{P}$ and $\hat{P}_\mu$ are the monopole pairing operator and the quadrupole pairing operator, respectively. Though the theory itself is not bound to any particular form of Hamiltonian, the advantage of using such a separable-force Hamiltonian is that the role of each interaction is well known and, therefore, the interpretation of the numerical result becomes easier. The interaction strengths are determined as follows: The strength of the quadrupole-quadrupole interaction χ is adjusted by the self-consistent relation such that the input quadrupole deformation ε_2 and the one resulting from the HFB (Hartree-Fock-Bogolyubov) procedure coincide with each other [13]. The

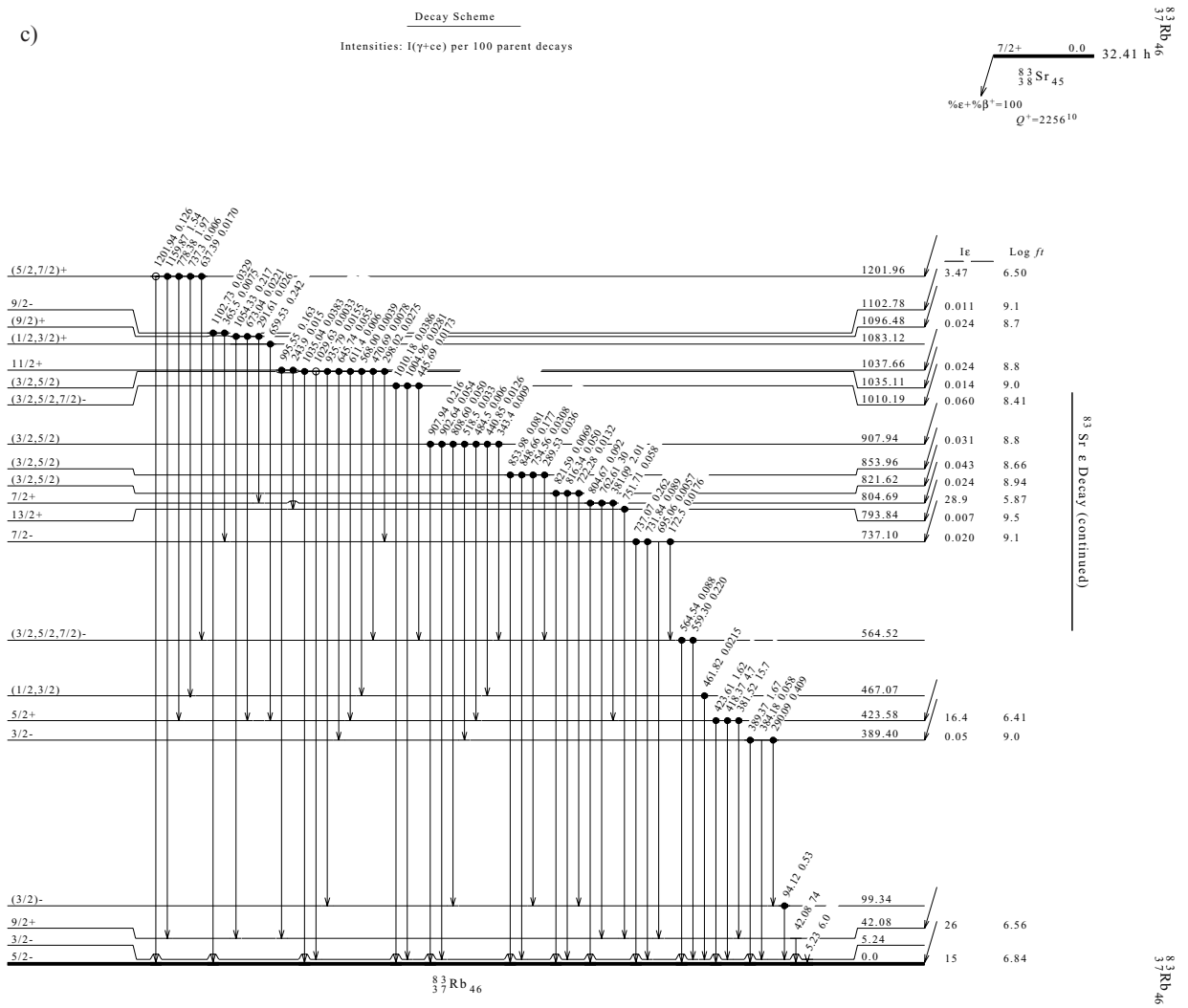

Fig. 2. Continued.

monopole pairing strength constant is adjusted to give the known energy gap

$$G_{\mathrm{M}} = \left[20.21 \mp 13.13\frac{N-Z}{A}\right] \cdot A^{-1}, \tag{5}$$

where "−" is for neutrons and "+" for protons. Finally the quadrupole pairing strength G_{Q} is simply assumed to be proportional to G_{M}

$$\left(\frac{G_{\mathrm{Q}}}{G_{\mathrm{M}}}\right)_{\mathrm{n}} = \left(\frac{G_{\mathrm{Q}}}{G_{\mathrm{M}}}\right)_{\mathrm{p}} = \gamma. \tag{6}$$

The proportionality constant γ is chosen as 0.20 for all the bands calculated in the present work.

The weights f_k in eq. (1) are determined by diagonalizing the Hamiltonian $\hat{H}$ in the basis given by eq. (3) as outlined in ref. [13]. The projection of good angular momentum onto each intrinsic state generates the rotational band associated with this intrinsic configuration $|\varphi_k\rangle$. For example, $\hat{P}^I_{MK} a^+_{\mathrm{p}}|0\rangle$ will produce a one-quasiproton band. The energies of each band are given by the normalized diagonal elements according to ref. [10]. A diagram in which $E_k(I)$ for various bands are plotted against spin I is referred to as a band diagram [13]. The lowest eigenvalue of the Hamiltonian for a given spin is named the yrast energy, and can be compared with the experiment. In this paper, we decide to compare the experimentally observed positive-parity yrast states and negative-parity ground-state band of ^{83}Rb with the predictions of the PSM.

The projected shell model has at least two advantages by this token: 1) The procedure of angular-momentum coupling, which must be done troublesomely in the conventional shell model, is done automatically by the projector irrespective of the number of quasiparticles (qp) involved. 2) It allows us to choose various multi-qp bases according to the physical importance. Unfortunately, our present computer code assumes axial symmetry, so that we cannot investigate those γ-deformed nuclei quantitatively [15]. The model has achieved considerable success when it was applied to the rare-earth region where the nucleus is well-deformed. In this paper, we try to apply this

model to the $A \sim 80$ region and to show the potential of this model via the study of the low- and high-spin states of ^{83}Rb.

3.2 Calculations and comparison with experimental results

In our calculations, the following formulae are used to calculate the pairing gap parameters $\Delta_{\rm p}$ and $\Delta_{\rm n}$ [16]:

$$\Delta_{\rm p} = \frac{1}{4}\big\{B(N,Z-2) - 3B(N,Z-1) + 3B(N,Z) - B(N,Z+1)\big\}, \quad (7)$$

$$\Delta_{\rm n} = \frac{1}{4}\big\{B(N-2,Z) - 3B(N-1,Z) + 3B(N,Z) - B(N+1,Z)\big\}, \quad (8)$$

the values of the total nuclear binding energy B are taken from ref. [17]. The results are $\Delta_{\rm p} = 1.8\,$MeV and $\Delta_{\rm n} = 1.08\,$MeV. The spin-orbit force parameters, κ and μ, appearing in the Nilsson potential are taken from the compilation of Zhang *et al.* [18] which is a modified version of Bengtsson and Ragnarsson [19] and has been fitted to the latest experimental data. It is supposed to apply over a sufficiently wide range of shells. These κ and μ are different for different major shells (N-dependent). According to total Routhian surface (TRS) calculations for the positive-parity states [6], at very low frequencies, the nucleus ^{83}Rb is calculated to be weakly deformed and very γ-soft, with a quadrupole deformation of about $\beta_2 = 0.13$ (equivalent to $\varepsilon_2 = 0.117$) and a triaxiality parameter of $\gamma = +17\,^\circ$. At a rotational frequency of 0.486 MeV (about spin $23/2^+$), a second minimum occurs which represents a well-deformed near-oblate shape with $\beta_2 = 0.25$ (equivalent to $\varepsilon_2 = 0.225$) and $\gamma = -66\,^\circ$. This second minimum persists up to high rotational frequencies. Therefore, we take quadrupole deformations equal to $\varepsilon_2 = 0.117 (5/2^+ \leq I < 23/2^+)$ and $\varepsilon_2 = -0.225 (I \geq 23/2^+)$, respectively, to calculate the positive-parity yrast states. The hexadecapole deformation parameter $\varepsilon_4 = 0.007$ is taken from the compilation of Möller *et al.* [17]. In the calculations, the configuration space is constructed by selecting the qp states close to the Fermi energy in the $N = 4$ ($N = 4$) major shell for neutrons (protons) and forming multi-qp states from them. The comparison of the experimentally observed positive-parity yrast levels of ^{83}Rb with the predictions of the PSM is given in fig. 3. The experimental $5/2^+, 7/2^+, 9/2^+, 11/2^+$ and $13/2^+$ levels have been taken from the present measurement, the rest have been taken from the in-beam study of the nucleus ^{83}Rb by Döring *et al.* [6]. In fact the $9/2^+$-$13/2^+$ ($5/2^+$-$13/2^+$) levels had also been observed in the in-beam work by Döring *et al.* [6] and Gast *et al.* [5]. The fair agreement of experimental and calculated level energies above the $21/2^+$ state indicates the alignment of a $g_{9/2}$ neutron pair in ^{83}Rb which drives the nucleus from a weakly deformed near-prolate shape to a medium deformed near-oblate shape. The reproduction of the relatively low-lying states ($5/2^+ \leq I < 23/2^+$) is not so satisfactory. This is because our present computer code assumes that the nucleus ^{83}Rb is axially symmetric. But we still find that the ordering of all calculated levels agrees with that of the experimental ones, especially the ordering of the 5/2, 7/2, 9/2 positive-parity yrast states, the so-called anomalous coupling states. From our calculations, it can be predicted that the $1/2^+$ and $3/2^+$ levels lie between the $11/2^+$ and $17/2^+$ levels, and the $19/2^+$ level lie above the $21/2^+$ level; it is expected that some experiments will confirm it in future.

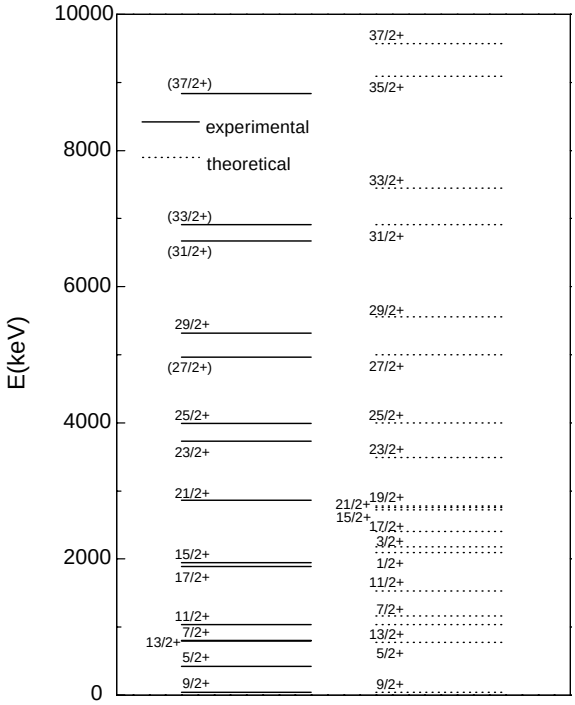

Fig. 3. Projected shell model calculations for positive-parity yrast states in ^{83}Rb compared with the experimental data.

In the negative-parity ground-state band calculations, the configuration space is constructed by selecting the qp states close to the Fermi energy in the $N = 4$ ($N = 3$) major shell for neutrons (protons) and forming multi-qp states from them. The negative-parity ground-state band (the $5/2^-$-$13/2^-$ levels are the yrast states), calculated also for a $\varepsilon_2 = 0.117$ deformation parameter, seems to give the best reproduction of the experiment. The theoretical energy difference $E(I) - E(I-1)$ of the negative-parity ground-state band is compared with the experimental data as shown in fig. 4. The experimental $5/2^-$, $7/2^-$ and $9/2^-$ levels have been taken from the present measurement, the rest have been taken from ref. [5]. In fact the $5/2^-$-$9/2^-$ levels had also been observed in the in-beam work by Gast *et al.* [5]. In the projected shell model calculation, by taking a quadrupole deformation $\varepsilon_2 = 0.117$ and a hexadecapole deformation $\varepsilon_4 = 0.007$, the ground-state spin and parity of ^{83}Rb were calculated to be $5/2^-$, which is consistent with the experimental results. The nucleus ^{83}Rb has been calculated to be almost spherical in its $5/2^-$ ground-state with a small quadrupole deformation of $\beta_2 = 0.071$ when a finite-range droplet macroscopic model

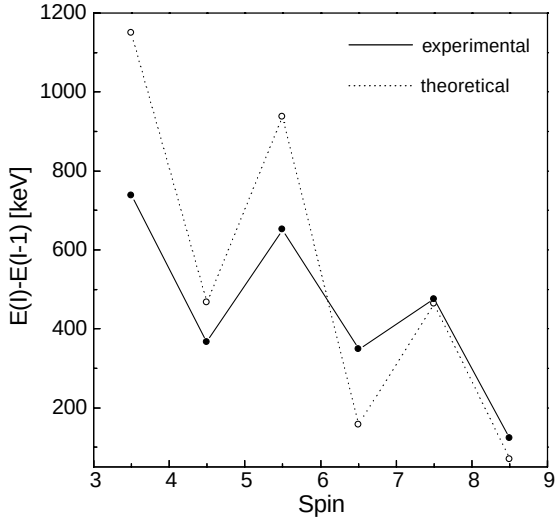

Fig. 4. The theoretical energy difference $E(I) - E(I-1)$ of the negative-parity band based on the g.s. $5/2^-$ is compared with experiment.

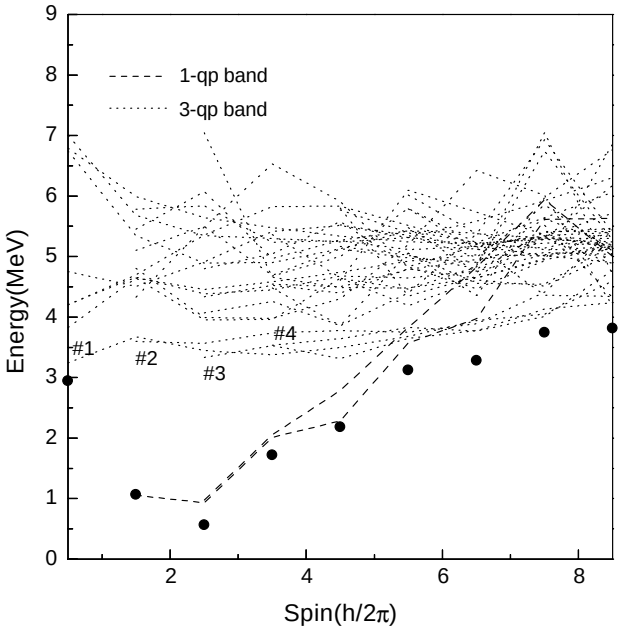

Fig. 5. A band diagram calculated for the negative-parity band in ^{83}Rb based on the $5/2^-$ ground state (filled circles). Different multi- (1-qp and 3-qp) bands are shown in different line types. All the results(filled circles included) are extracted from PSM calculations.

and a folded-Yukawa single-particle microscopic model are used [17]. But when we use this quadrupole deformation to calculate the negative-parity yrast states, the fit is rather bad for these experimental data. So in the present work the deformation of this ground-state band is tentatively assigned as $\varepsilon_2 = 0.117$, and this is in accordance with the work of Maharana *et al.* [20], in which the ground state of ^{83}Rb has been calculated using the relativistic mean-field theory.

In fact in the present example of ^{83}Rb, where the negative-parity band is based on the $5/2^-$ ground state, one finds that the neutron Fermi energy lies between the $K = 5/2$ and $K = 7/2$ qp states of the intruder $1g_{9/2}$ subshell and the proton Fermi energy lies between the $K = 3/2$ and $K = 5/2$ qp states of the $1f_{5/2}$ subshell. Therefore, orbitals around these levels are physically most important. To build a multi-qp basis, all neutron qp states of the intruder $1g_{9/2}$ subshell are selected, from which 10 neutron 2-qp states are formed. Similarly, the $K = 3/2$ and $K = 5/2$ proton qp states of the $1f_{5/2}$ subshell are selected. Furthermore, 40 3-qp states are constructed from these neutron 2-qp and proton 1-qp states. Consequently, the dimension of our configuration space finally becomes $42(40 + 2)$. The shell model configuration space is constructed by projecting each of these multi-qp states onto a good angular momentum and the Hamiltonian is diagonalized in this space. The band diagram as mentioned in section 3.1 is shown in fig. 5. Filled circles in this figure represent the negative-parity g.s. band numbers, which are obtained from the final diagonalization procedures (band mixing) [21] and also have been shown in fig. 4. It is this kind of diagrams which one can conveniently use to extract physics out of the numerical results [13]. In the lowest spin region ($3/2 \leq I \leq 11/2$), the yrast states are represented by the 1-qp band, indicating that the 3-qp states have little effect on the yrast states in this spin range. The $I = 1/2$ state has not yet certainly been observed in the experiment, so it will not be discussed in the present work. At spin $I \approx 11/2$, the first band crossing is seen to take place. In the present case, there are accidentally four closely lying (3-qp) bands which cross the 1-qp band and after $I \geq 15/2$ there are some other 3-qp bands which come down in energy and contribute to the negative-parity band based on the $5/2^-$ ground-state, thus complicating the structure. We thus want to know the configurations of these four closely lying (3-qp) bands. We see that the band #3(#2) is a 3-qp band with $K_{\mathrm{n}_1} = 5/2$ and $K_{\mathrm{n}_2} = -7/2$ coupled to $K = -1$ and then coupled with $K_{\mathrm{p}} = -3/2(K_{\mathrm{p}} = 5/2)$ to total $K = -5/2(K = 3/2)$ while band #1(#4) is a 3-qp band with $K_{\mathrm{n}_1} = 5/2$ and $K_{\mathrm{n}_2} = -7/2$ coupled to $K = -1$ and then coupled with $K_{\mathrm{p}} = 3/2(K_{\mathrm{p}} = -5/2)$ to total $K = 1/2(K = -7/2)$.

4 Summary

In summary, the decay of ^{83}Sr has been reinvestigated using γ singles and a γ-γ-t coincidence measurement. The number of γ transitions assigned to the ^{83}Sr decay has been expended from 102 to 196. Nineteen new levels of ^{83}Rb have been added to the old level scheme and eight formerly adopted levels are denied by the present study. New results on branching ratio, $\log ft$ value and spin-parity assignments have been obtained. In addition, the structure of excited positive-parity yrast states and the negative-parity ground-state band of ^{83}Rb has been discussed in the framework of the projected shell model, and the best reproduction of the experiment has been given by this model.

The authors would like to thank the operating staff at the cyclotron in Shanghai Institute of Nuclear Research. This work was supported by the National Natural Science Foundation of China under Grant No. 19635030, the Chinese Academy of Sciences under Grant No. KJ-952-S1-420, and the Natural Science Foundation of Shanghai under Grant No. 00ZA14078.

References

1. R.C. Etherton, L.M. Beyer, W.H. Kelly, D.J. Horen, Phys. Rev. **168**, 1249 (1968).
2. R. Broda, A.Z. Hrynkiewicz, J. Styczeń, W. Walus, Nucl. Phys. A **216**, 493 (1973).
3. A. Grütter, Int. J. Appl. Radiat. Isot. **33**, 456 (1982).
4. J. Müller, Nuclear Data Sheets **49**, 579 (1986).
5. W. Gast, K. Dey, A. Gelberg, U. Kaup, F. Paar, R. Richter, K.O. Zell, P. von Brentano, Phys. Rev. C **22**, 469 (1980).
6. J. Döring, G.D. Johns, R.A. Kaye, M.A. Riley, S.L. Tabor, Phys. Rev. C **60**, 014314 (1999).
7. X.H. Yu, S.H. Shi, J.H. Gu, J.Y. Liu, W.X. Li, J.P. Zeng, J.Q. Tian, Y. Li, J.Z. Zhou, High Energy Phys. Nucl. Phys. (in Chinese) **22**, 1082 (1998).
8. D. Mehta, M.L. Garg, J. Singh, N. Singh, T.S. Cheema, P.N. Trehan, Nucl. Instr. Meth. Phys. Res. A **245**, 447 (1986).
9. A.H. Wapstra, G. Audi, Nucl. Phys. A **432**, 1 (1985).
10. K. Hara, Y. Sun, Nucl. Phys. A **529**, 445 (1991).
11. K. Hara, Y. Sun, Nucl. Phys. A **531**, 221 (1991).
12. K. Hara, Y. Sun, Nucl. Phys. A **537**, 77 (1992).
13. K. Hara, Y. Sun, Int. J. Mod. Phys. E **4**, 637 (1995).
14. C.G. Andersson, G. Hellström, G. Leander, I. Ragnarsson, S. Åberg, J. Krumlinde, S.G. Nilsson, Z. Szymański, Nucl. Phys. A **309**, 141 (1978).
15. M.A. Rizzutto, E.W. Cybulska, L.G.R. Emediato, N.H. Medina, R.V. Ribas, K. Hara, C.L. Lima, Nucl. Phys. A **569**, 547 (1994).
16. A. Bohr, B.R. Mottelson. *Nuclear Structure*, Vol. **1** (Benjamin, New York, Amsterdam, 1969) p. 169.
17. P. Möller, J.R. Nix, W.D. Myers, W.J. Swiatecki, At. Data Nucl. Data Tables **59**, 185 (1995).
18. Jing-ye Zhang, A.J. Larabee, L.L. Riedinger, J. Phys. G **13**, L75 (1987).
19. T. Bengtsson, I. Ragnarsson, Nucl. Phys. A **436**, 14 (1985).
20. J.P. Maharana, Y.K. Gambhir, Phys. Rev. C **54**, 2404 (1996).
21. Y. Sun, K. Hara, Comp. Phys. Comm. **104**, 245 (1997).